STANDARDS

A Deep Learning Approach for State of Health Estimation of Lithium-Ion Batteries Based on Differential Thermal Voltammetry

YEONHO CHOI[1], **JAEJUNG YUN**[1], **(Member, IEEE), AND PAUL JANG**[2], **(Member, IEEE)**

[1]School of Electrical Engineering, Chungbuk National University, Cheongju 28644, South Korea
[2]Department of Energy and Electrical Engineering, Tech University of Korea, Siheung 15073, South Korea

Corresponding author: Paul Jang (paul716@tukorea.ac.kr)

ABSTRACT Accurately estimating the actual capacity of the battery is crucial for stable battery operation and user safety. This paper combined feature extraction through differential thermal voltammetry analysis and long short-term memory for accurate state of health estimation. First, differential thermal voltammetry curves according to battery degradation were extracted for various cathode materials. Then, health indicators are collected from the differential thermal voltammetry curve for deep learning-based state of health estimation. In particular, to improve the state of health estimation performance, the integral value of the differential thermal voltammetry curve through the specific voltage ranges was additionally introduced along with the peak and valley. Second, the correlation between the extracted health indicators and capacity was analyzed using Pearson correlation analysis. Finally, a framework was developed to estimate the state of health of the battery using high-quality health indicators as inputs to the long short-term memory model. The state of health estimation performance of the proposed algorithm, which reflected the integral value of the differential thermal voltammetry curve, was compared with the case that did not reflect. From the result, the mean absolute error decreased by 11.6% and the root mean square error by 10.01% for the two battery data sets.

INDEX TERMS Lithium-ion battery, state of health, differential thermal voltammetry, long short-term memory, battery management system.

I. INTRODUCTION

Lithium-ion batteries have been widely used as energy storage devices in applications such as electric vehicles and smart grids [1], [2], [3]. However, their performance decreases during cycling, which increases the risk of fire and explosion accidents [4], [5], [6]. Therefore, it is essential to estimate and monitor the state of health (SOH) of the battery for efficient and stable usage. Conventional methods for estimating battery SOH can be roughly divided into two groups: 1) model-based method and 2) data-driven method.

The associate editor coordinating the review of this manuscript and approving it for publication was Enamul Haque.

For the model-based method, equivalent circuit models or electrochemical models are used to analyze the dynamic characteristics of the battery. Afterward, the battery capacity or internal resistance is set as a state variable, and the SOH is estimated using a filter or observer algorithm [7], [8], [9]. Since SOH estimation accuracy is highly dependent on the model accuracy, these methods require professional knowledge of battery modeling.

Recently, with the advancement of computing power and data collection techniques, SOH estimation using data-driven based on battery operation data has been widely studied [10], [11]. The data-driven method extracts health indicators (HIs) reflecting capacity fade from experiment data and then

estimates SOH using a data mining algorithm [12], [13]. Because this method estimates SOH based on data, it does not require knowledge of complex electrochemical mechanisms as in model-based methods. However, because extracted HIs significantly impact SOH estimation performance, it is crucial to decide which HI to use for successful estimation.

HIs extracted directly from battery voltage, current, and temperature information, such as constant current (CC) charging time, constant voltage (CV) charging time, and area of the data curve, can be easily obtained from the raw battery data [14], [15], [16]. Nevertheless, these HIs cannot effectively explain the internal degradation mechanisms of the battery.

Meanwhile, battery degradation mechanisms can be examined through incremental calculation-based HIs, which can be obtained by further processing battery raw data [17], [18], [19], [20], [21]. Incremental capacity analysis (ICA) and differential voltage analysis (DVA) are representative examples of incremental calculation-based HI. In this way, HIs extracted from incremental capacity (IC) and differential voltage DV curves can help explain battery aging mechanisms and estimate SOH more accurately [20], [21].

Recently, differential thermal voltammetry (DTV) has also been proposed as an effective method to explain the degradation mechanism of batteries. Similar to ICA and DVA, DTV analysis can capture changes in the curve due to degradation, and the result can be used as HI. In existing DTV-based SOH estimation studies, the positions and heights of the peak and valley of the curve were extracted as HI and used as input for the deep learning algorithm [22], [23], [24], [25], [26]. Reference [22] extracted the positions and heights of peaks and valleys from the DTV curve as HIs and estimated SOH through Gaussian process regression (GPR). Reference [23] extracted the positions and heights of peaks and valleys from the DTV curve as HIs and estimated SOH using long short-term memory (LSTM). Additionally, the hyper-parameters of the model were selected through Bayesian optimization. Reference [24] extracted HIs through various analysis techniques such as ICA, DTV, and terminal voltage characteristics and then estimated SOH using LSTM. However, in existing literature, only the position and height of the peak and valley of the DTV curve were used. Although studies of other incremental calculation-based HI have shown that the change in curve area over the cycle is highly correlated with capacity degradation [27], [28], this approach has not yet been attempted in DTV research.

From the above perspective, this study aims to demonstrate that SOH estimation performance can be improved by utilizing the integral value of the DTV curve according to the specific voltage ranges, in addition to the peak and valley of the DTV curve, as input to the deep learning algorithm for SOH estimation. Specifically, the DTV analysis is implemented using experimental data from various cathode material batteries. An apparent DTV curve is obtained through the Savitzky-Golay (SG) filter, and HIs highly correlated with SOH are extracted through Pearson correlation

TABLE 1. Main specifications of SLPB533459H4.

Parameter	Value
Cathode material	LCO/NCO
Anode material	Graphite
Nominal capacity	740 mAh
Nominal voltage	3.7 V
Discharge cutoff voltage	2.7 V
Charge cutoff voltage	4.2 V
Weight	19.5±0.5g

analysis. In addition to the peak and valley obtained from the DTV curve, the integral value according to the specific voltage ranges is input into the LSTM to verify the SOH estimation performance. The SOH estimation performance of the proposed algorithm reflecting the integral value of the DTV curve was compared with the case that did not reflect. As a result, the error was significantly reduced, confirming the validity of the proposed SOH estimation algorithm.

II. DIFFERENTIAL THERMAL VOLTAMMETRY-BASED HEALTH INDICATOR EXTRACTION
A. BATTERY DEGRADATION DATASETS
This paper used two battery data sets to test the feasibility of DTV-based HIs extraction. Most existing literature that extracted HIs from DTV used battery data sets provided by the University of Oxford and NASA [22], [23], [24], [25], [26]. However, lithium-ion batteries exhibit various characteristics depending on the composition of the cathode material, which may cause the shape of the DTV curve to vary. Therefore, in this study, deterioration data for batteries that were not previously used were additionally collected to verify whether DTV analysis can be applied to various batteries.

The first dataset is the battery degradation dataset from the University of Oxford [29]. The battery used in the experiment was a pouch-type battery SLPB533459H4 manufactured by Kokam. The battery consists of an anode made of graphite and a cathode combined with lithium cobalt oxide (LCO) and lithium nickel cobalt oxide (NCO). Detailed specifications are shown in Table 1. Charging and discharging were performed using a Bio-logic MPG 205 battery tester and tested in a chamber maintained at 40°C. The battery was charged at a 2C rate in a chamber at 40°C and discharged using a dynamic discharge profile for degradation. After performing the degradation profile 100 times, battery degradation data is collected by applying charging and discharging at a rate of 1C. In other words, battery data was collected every 100 degradation cycles. Fig. 1 shows the evolution in capacity, voltage, and temperature due to the degradation of the LCO/NCO battery from data collected when a 1C charging and discharging profile is applied every 100 degradation cycles.
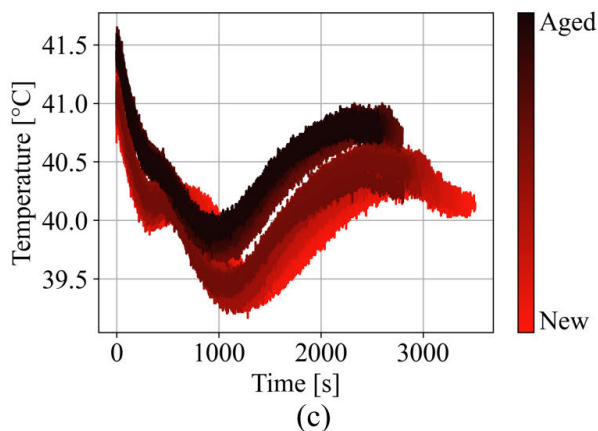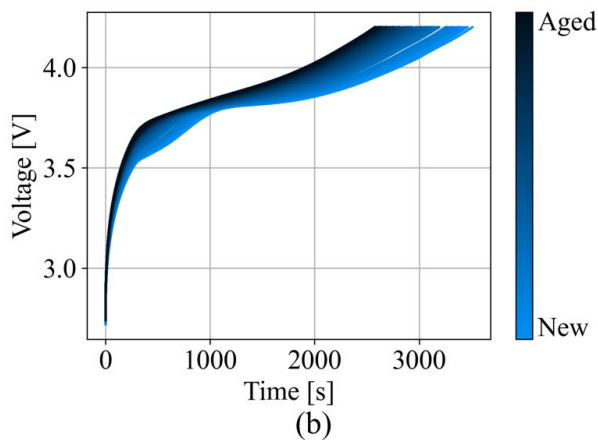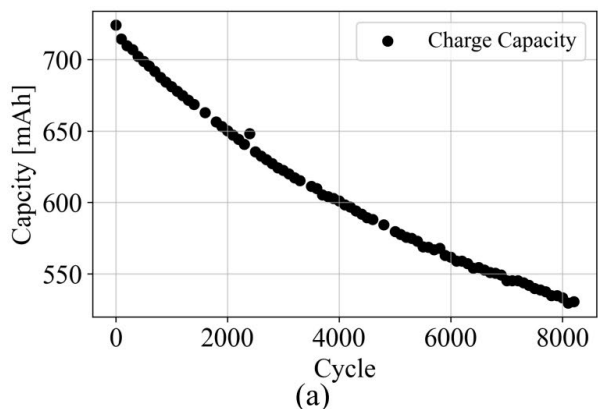
FIGURE 1. Evolution of the capacity, voltages, and surface temperatures of LCO/NCO battery throughout the degradation process: (a) charge capacity, (b) terminal voltage, (c) surface temperature.

The second data set is battery degradation data tested in the laboratory of the authors. The battery used in the experiment was cylindrical INR 18650-25R manufactured by Samsung. The battery consists of a graphite anode and a cathode combined with lithium nickel cobalt manganese oxides (NCM) and lithium nickel cobalt aluminum oxide (NCA). Detailed specifications are shown in Table 2. As shown in Fig. 2, charging and discharging were carried out using the Bio-logic BCS 815 battery tester, and the experiment was conducted in a constant temperature-humidity chamber maintained at a temperature of 25°C and humidity of 65%.

TABLE 2. Main specifications of INR 18650-25R.

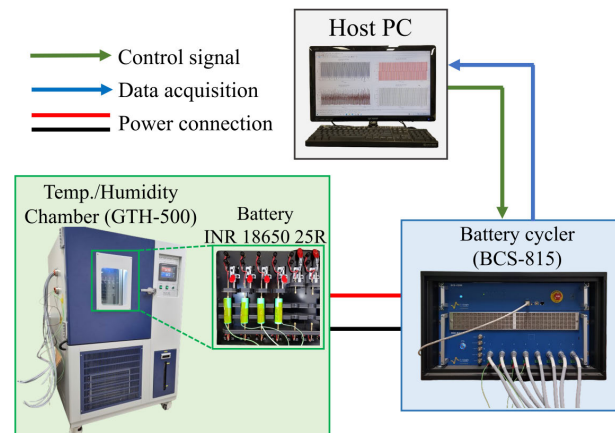| Parameter	Value
Cathode material	NCM/NCA
Anode material	Graphite
Nominal capacity	2500 mAh
Nominal voltage	3.6 V
Discharge cutoff voltage	2.5 V
Charge cutoff voltage	4.2 V
Weight	45.0g

FIGURE 2. Battery test bench, which consists of host PC, battery cycler, battery, and temperature-humidity chamber.

Battery cells were degraded through CC-CV charging and CC discharging at a 0.5C rate, with an idle period of 1 hour between charging and discharging. Battery data was collected for voltage, temperature, and capacity at every cycle. Fig. 3 shows the evolution in capacity, voltage, and temperature due to the degradation of the NCM/NCA battery.

Fig. 1 and Fig. 3 show that battery capacity and CC charging time decrease as the number of cycles increases, whereas surface temperature increases due to the influence of internal resistance.

B. DIFFERENTIAL THERMAL VOLTAMMETRY CURVE EXTRACTION

The DTV curve was extracted throughout the battery degradation data. DTV can be obtained through changes in battery surface temperature according to terminal voltage during CC charging and is expressed as follow

$$DTV_k = \frac{dT_k}{dV_k} = \frac{T_k - T_{k-1}}{V_k - V_{k-1}} = \frac{T_k - T_{k-1}}{t_k - t_{k-1}} \bigg/ \frac{V_k - V_{k-1}}{t_k - t_{k-1}} \tag{1}$$

where T_k and V_k denote the battery surface temperature and terminal voltage measurements at time t_k, respectively. Generally, temperature and voltage data in actual applications contain sensor noise, which significantly affects the accuracy of the DTV curves. In particular, battery analysis techniques
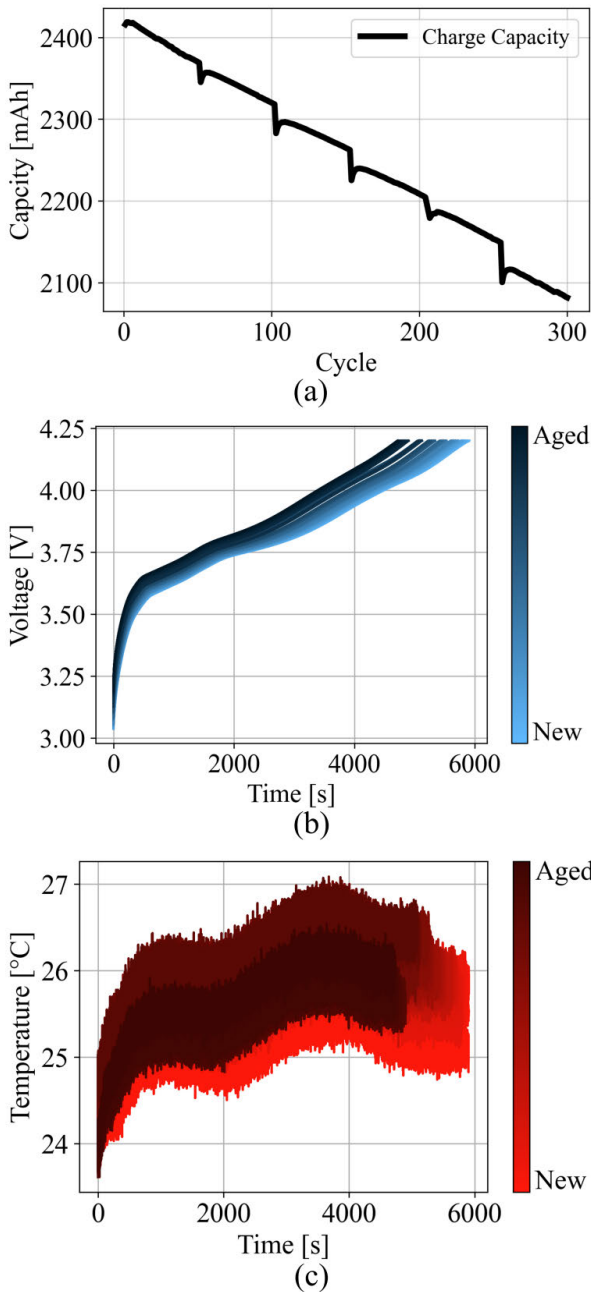
FIGURE 3. Evolution of the capacity, voltages, and surface temperatures of NCM/NCA battery throughout the degradation process: (a) charge capacity, (b) terminal voltage, (c) surface temperature.

based on incremental calculations, such as ICA and DTV, are vulnerable to noise due to differential calculations. Fig. 1(c) and Fig. 3(c) show that the battery surface temperature contains a huge noise component. Therefore, noise must be removed to extract the DTV curve accurately. If the selected time interval for extracting the DTV curve is too small, it is vulnerable to noise. On the other hand, if it is too large, the information in the data cannot be appropriately reflected. Therefore, through trial and error, the optimal time interval, $t_k - t_{k-1}$, was derived as 15 seconds in this study. Then, the data were smoothed by applying the SG filter to obtain apparent
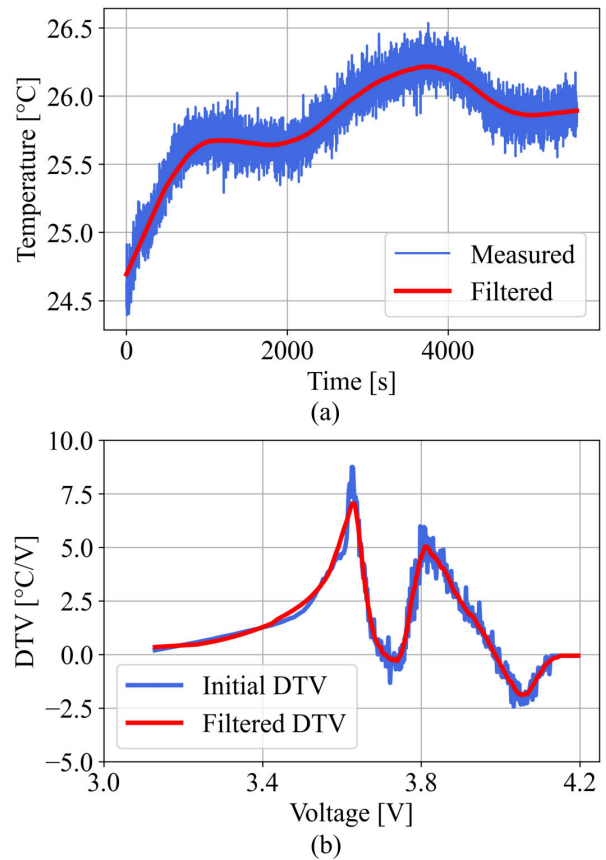

FIGURE 4. Filtered battery surface temperature and DTV curve: (a) comparison of the surface temperature curves before and after smoothing by SG filter, (b) comparison of DTV curve after surface temperature smooth and DTV curve smoothed by SG filter.

temperature and DTV curves. Although this paper does not introduce the SG filter algorithm in detail, it has been widely used for filtering DTV curves [30], [31], and the detailed algorithm can also be found in [32].

Fig. 4 shows the temperature and DTV curves when the noise is removed through the SG filter. Fig. 4(a) shows the raw temperature data and the smoothed curve by the SG filter. The DTV curve calculated based on the filtered temperature data is shown in Fig. 4(b). The calculated DTV curve was also smoothed using an SG filter for accurate identification.

C. HEALTH INDICATOR EXTRACTION
Fig. 5(a) and Fig. 5(b) show the evolution of the DTV curve due to the degradation in the LCO/NCO battery and the NCM/NCA battery, respectively, when an SG filter removes noise. In the LCO/NCO battery, one valley and two peaks can be identified, and in the NCM/NCA battery, two peaks and two valleys can be identified. As seen in the figure, as the battery degrades, the voltages where the peak and valley occur change. In addition, as the DTV value gradually changes, the integral value of the DTV curve in the specified voltage range also changes, as shown in Fig. 6.
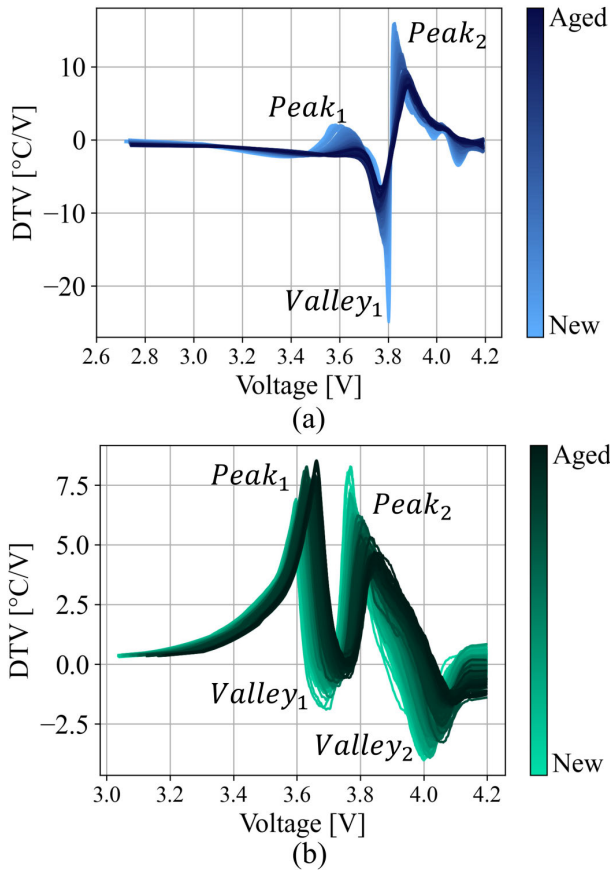
FIGURE 5. The evolution of the DTV curve throughout the battery degradation process: (a) LCO/NCO battery, (b) NCM/NCA battery.

FIGURE 6. Integral value of the DTV curve as a new health indicator: (a) LCO/NCO battery, (b) NCM/NCA battery.

The peak and valley of the DTV curve can be calculated as follows

$$\begin{cases} V_{peak} = V\big|_{\frac{dDTV}{dV_i}=0,\ and\ f(V_i)\geq f(V),\ V\in(V_{i-1}, V_{i+1})} \\ DTV_{peak} = f(V_{peak}) \end{cases} \quad (2)$$

$$\begin{cases} V_{valley} = V\big|_{\frac{dDTV}{dV_i}=0,\ and\ f(V_i)\leq f(V),\ V\in(V_{i-1}, V_{i+1})} \\ DTV_{valley} = f(V_{valley}) \end{cases} \quad (3)$$

where $f(\cdot)$, V_{i-1}, and V_{i+1} represent the mapping function between voltage and DTV, voltages at the previous and later sampling points, respectively. The integral value of the DTV curve over the specific voltage range can be calculated as

$$\int_{V_{lower}}^{V_{upper}} DTV(V)\, dV = \int_{V_{lower}}^{V_{upper}} \frac{dT}{dV}\, dV$$
$$= T(V_{upper}) - T(V_{lower}) = \Delta T \quad (4)$$

where V_{upper} and V_{lower} mean the upper and lower limits of the voltage range, respectively.

From (5), it can be seen that the integral value of the DTV curve according to the voltage range is calculated as the change in surface temperature. Fig. 6 shows a schematic representation of the peak, valley, and integral value of the DTV curve.

This study first derived the peak and valley voltage positions and DTV values to apply the proposed estimation
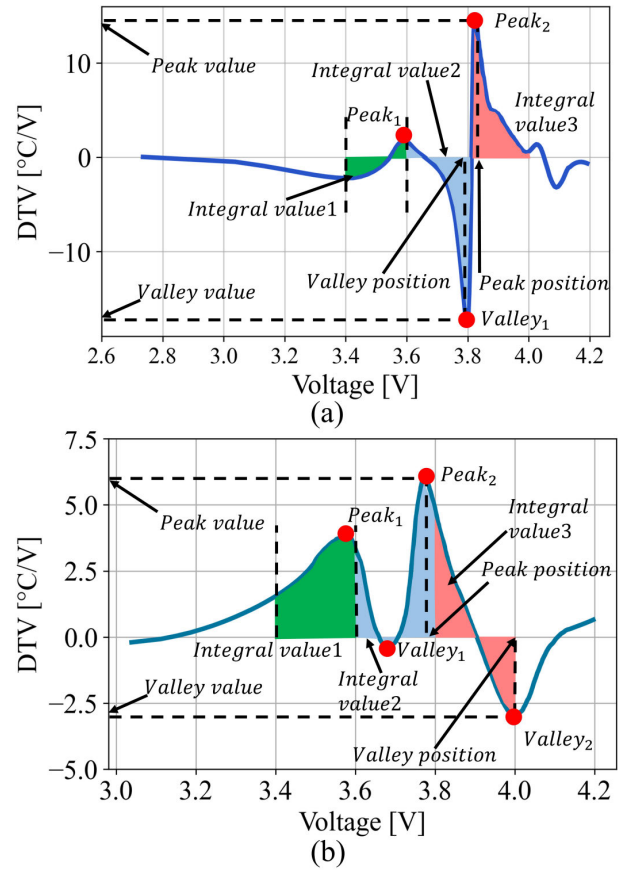
algorithm. The DTV curve of the battery data sets used in this study confirmed that the peak and valley exist within 3.4V to 4.0V. As the battery ages, the integral value of the DTV curve in this range will gradually change depending on the peak and valley values, and it can be inferred that it can be used as a HI that reflects battery aging characteristics. Therefore, to ensure that the integral value of the DTV curve proposed in this study is HI to reflect better battery aging characteristics, three integral values from 3.4V to 3.6V, 3.6V to 3.8V, and 3.8V to 4.0V were selected as parameters.

Fig. 7 and Fig. 8 show the extracted HIs of the LCO/NCO and NCM/NCA batteries, respectively. The subscript 'pos' represents the voltage position of the peak and valley, and the subscript 'val' represents the DTV value at the peak and valley. Additionally, integral value1, integral value2, and integral value3 indicate the integral values of the DTV curve for the voltage ranges of 3.4 to 3.6V, 3.6 to 3.8V, and 3.8 to 4.0V, respectively.

D. CORRELATION ANALYSIS

Pearson correlation analysis was conducted on the extracted HIs to ensure high accuracy and efficiency of SOH estimation. Through Pearson correlation analysis, the correlation between extracted HI and capacity can be quantitatively
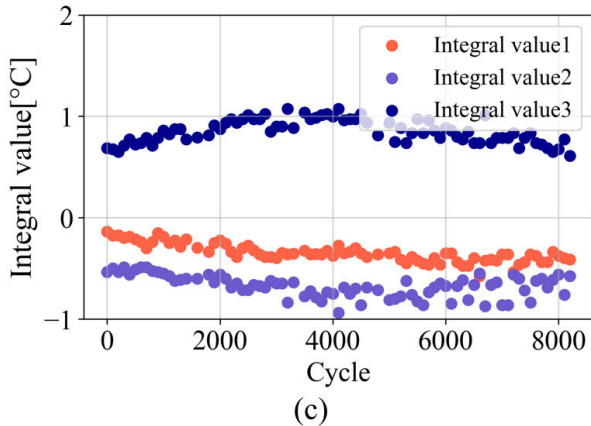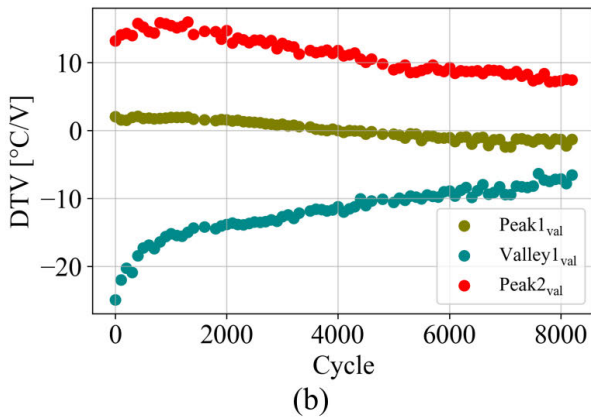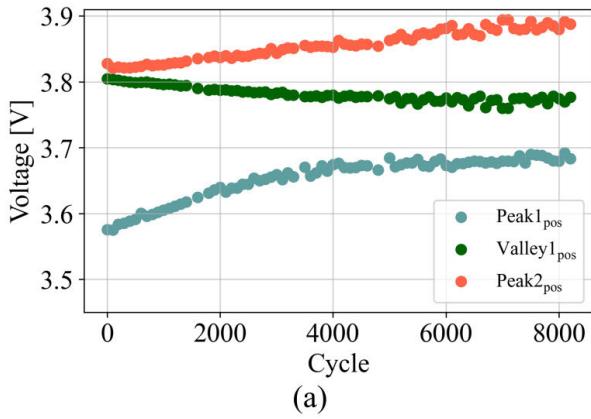
FIGURE 7. Extracted health indicators of LCO/NCO battery: (a) voltage position of peak and valley, (b) DTV value of peak and valley, (c) Integral value according to voltage range.
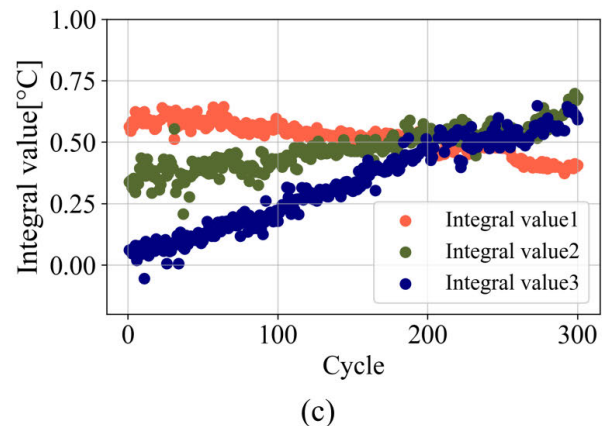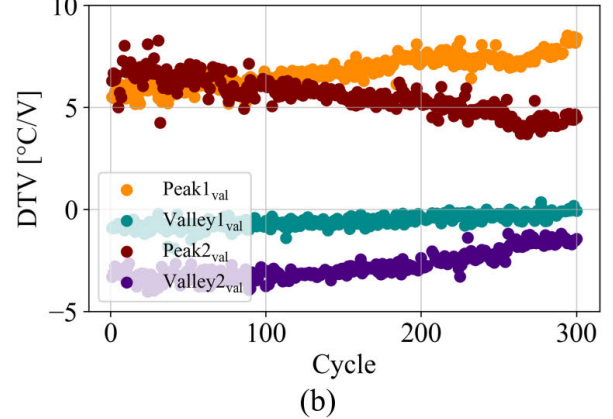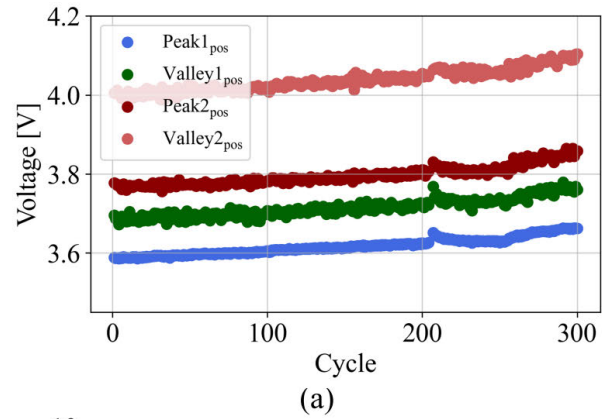

FIGURE 8. Extracted health indicators of NCM/NCA battery: (a) voltage position of peak and valley, (b) DTV value of peak and valley, (c) Integral value according to voltage range.

determined as follow

$$r_{xy} = \frac{\sum_{i=1}^{N}(x_i - \bar{x})(y_i - \bar{y})}{\sqrt{\sum_{i=1}^{N}(x_i - \bar{x})^2}\sqrt{\sum_{i=1}^{N}(y_i - \bar{y})^2}} \quad (5)$$

where N, x and y represent the data size and variables, respectively. $\bar{x}$ and $\bar{y}$ mean the average values of x and y. Fig. 9 shows the results of Pearson correlation analysis between the HIs and capacity calculated by (6). Most HIs have a high correlation with capacity. This study used high-quality HIs

with a correlation coefficient of 0.8 or higher as inputs for deep learning to ensure high accuracy of SOH estimation.

III. SOH ESTIMATION METHOD
A. LSTM MODEL STRUCTURE
In this paper, LSTM was used to estimate SOH. LSTM is a variant of RNN that solves RNN's long-term dependence problem, gradient vanishing and exploding. Fig. 10 shows the structure of LSTM. The forward propagation process of the LSTM unit at time t is as follows:

$$f_t = \sigma(W_{fx}x_t + W_{fh}h_{t-1} + b_f) \quad (6)$$
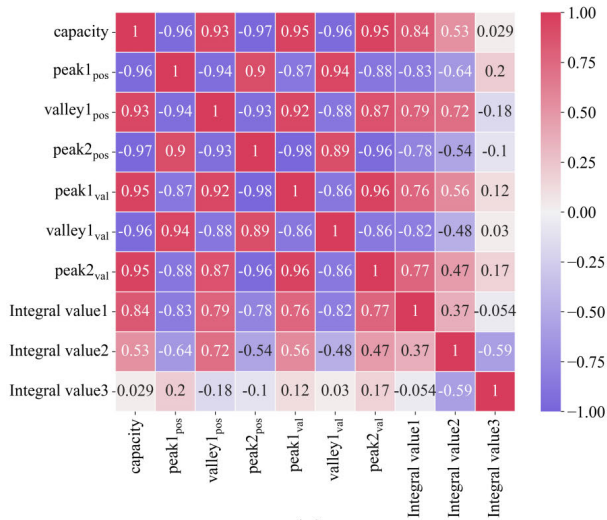
(a)

(b)

FIGURE 9. The correlation coefficient between extracted health indicators and capacity: (a) LCO/NCO battery, (b) NCM/NCA battery.

$$i_t = \sigma(W_{ix}x_t + W_{ih}h_{t-1} + b_i) \tag{7}$$

$$o_t = \sigma(W_{ox}x_t + W_{oh}h_{t-1} + b_o) \tag{8}$$

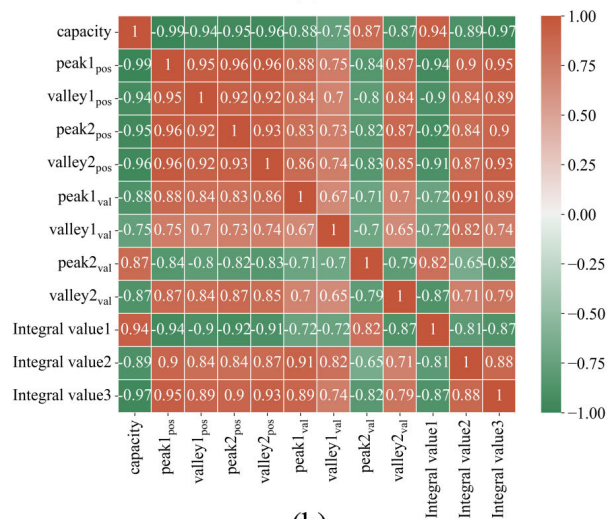$$C_t = f_t C_{t-1} + i_t \tanh(W_{cx}x_t + W_{ch}h_{t-1} + b_c) \tag{9}$$

$$h_t = o_t \times \tanh(C_t) \tag{10}$$

where f_t, i_t, and o_t are the forget, input, and output gates at time t, respectively. C_t is the cell state, and h_t is the hidden output. σ and *tanh* are sigmoid and hyperbolic tangent activation functions, respectively. W and b are weight and bias.

B. FRAMEWORK OF DIFFERENTIAL THERMAL VOLTAMMETRY-BASED SOH ESTIMATION

Fig. 11 shows the framework of the SOH estimation model combining DTV analysis and LSTM. The framework comprises four parts: data gathering, feature extraction, model construction, and SOH estimation. In the first part of the framework, battery terminal voltage, surface temperature,
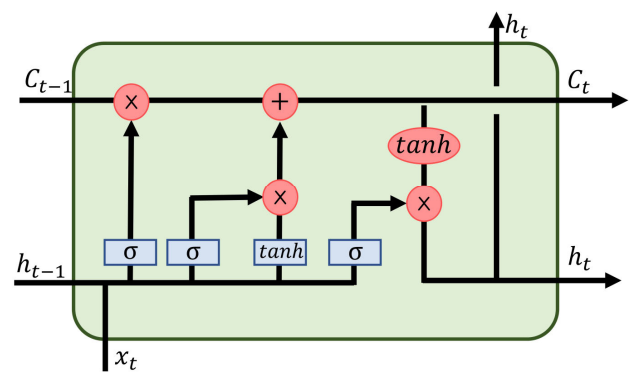

FIGURE 10. Structure of LSTM model.

and capacity are collected for DTV analysis. The second part extracts the DTV curve using the battery terminal voltage and surface temperature data. Additionally, HIs that reflect battery degradation are extracted utilizing the peak, valley, and integral values of the DTV curve. In the third part, Pearson correlation analysis is used to determine HIs that correlate highly with capacity degradation and are selected as input data for LSTM. Additionally, the dropout method is employed to mitigate model overfitting. The LSTM model utilizing the Adam optimizer is developed to expedite model convergence. In the last part, the estimated SOH and real SOH are compared using various evaluation indexes, and model performance is quantitatively evaluated.

IV. RESULT AND DISCUSSION
This section performs accuracy verification and error analysis of the SOH estimation model combining DTV and LSTM. First, the test setup for SOH estimation and the hyperparameters of the deep learning model are introduced. Second, the evaluation indexes to verify the SOH estimation model are introduced. Third, the SOH estimation performance of the conventional method using only the peak and valley of the DTV curve and the proposed method were compared. Additionally, to ensure accuracy even when the amount of data is small, performance was verified according to various split proportions of the dataset. Finally, a discussion of the proposed method and future research is provided.

A. TEST SETUP AND HYPERPARAMETERS
This study used PyTorch to build the deep learning-based SOH estimation model, utilizing the compute unified device architecture (CUDA) to accelerate computation. The version of PyTorch is 1.11.0, and the version of CUDA is 11.1. The workstation with an Intel i9 10940X CPU and Nvidia RTX 3090 D6X were used for SOH estimation.

Hyperparameters significantly affect the training speed, convergence, and accuracy of deep learning models. Hence, they must be optimally selected through debugging. The LCO/NCO battery has a small data size because data was measured every 100 cycles. However, the NCM/NCA battery has a large data size because data was measured every single cycle. Therefore, the hyperparameters for the optimal
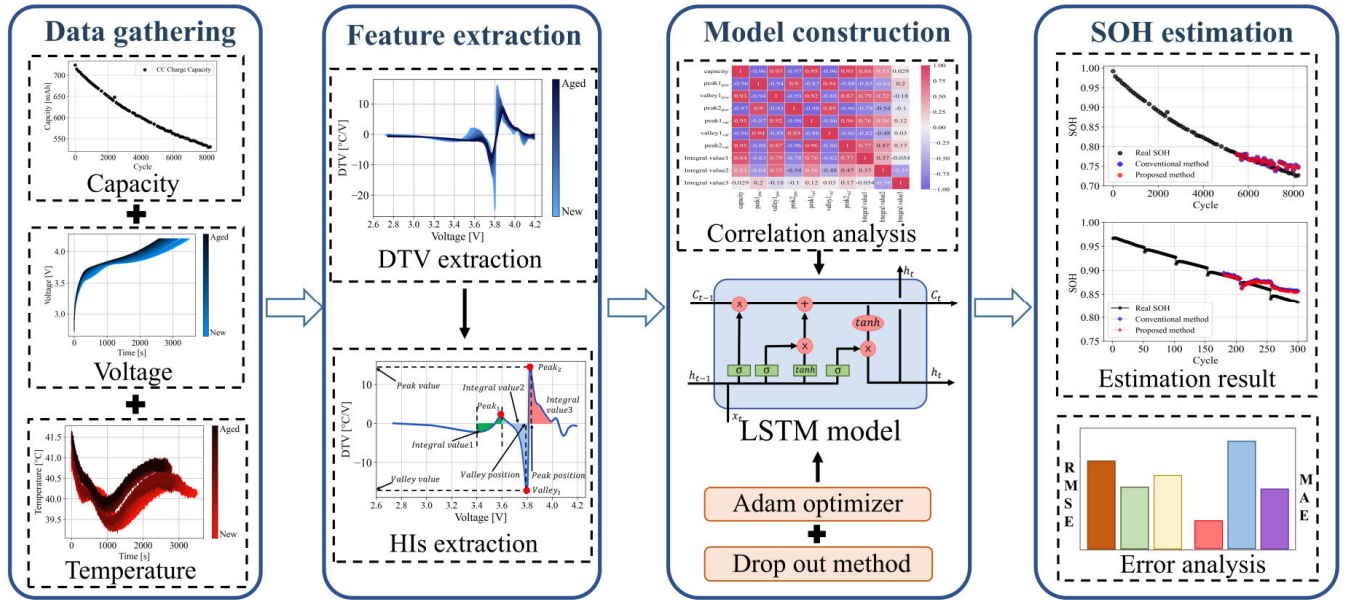
FIGURE 11. The framework of SOH estimation model combining DTV analysis and LSTM.

TABLE 3. Hyperparameters of deep learning model.

Hyperparameters	Value	
	LCO/NCO	NCM/NCA
Optimization method	Adam	Adam
Units of layers	128	128
Drop out	0.1	0.1
Batch size	2	32
Epoch	100	100
Learning rate	0.0012	0.003
Loss function	MSE	MSE

TABLE 4. Estimation error of the conventional method and the proposed method.

Battery type	Method	MAE	RMSE
LCO/NCO	Conventional	0.009978	0.01274
	Proposed	0.00882	0.01146
NCM/NCA	Conventional	0.01172	0.01415
	Proposed	0.01038	0.01288

of the LSTM was verified according to the split proportion of the dataset.

training speed and SOH estimation performance may differ for two battery datasets of different sizes. Table 3 shows the hyperparameters of the deep learning model used in this research.

B. EVALUATION INDEX

Root mean square error (RMSE) and mean absolute error (MAE) were used to quantitatively evaluate the SOH estimation results. RMSE and MAE can be calculated as

$$RMSE = \sqrt{\frac{1}{N}\sum_{i=1}^{N}(SOH_{i,est} - SOH_{i,real})} \quad (11)$$

$$MAE = \frac{1}{N}\sum_{i=1}^{N}\left|SOH_{i,est} - SOH_{i,real}\right| \quad (12)$$

where N represents the size of the data, $SOH_{i,est}$ represents the estimated SOH value, and $SOH_{i,real}$ means the real SOH value. In this research, the performance of the LSTM model was compared using RMSE and MAE, and the performance

C. SOH ESTIMATION RESULT

This subsection verifies the performance of the proposed deep learning-based SOH estimation model. Deep learning models learn patterns from training data and estimate states, and the quantity and quality of training data significantly impact state estimation performance. This paper uses the Pearson correlation analysis technique to quantitatively evaluate the quality of HIs based on the integral value of the DTV curve. As a result of correlation analysis, it was confirmed that the integral value of different DTV curves in a specific voltage range has a high correlation with battery capacity. SOH estimation performance can be improved by additionally utilizing HIs, which are highly correlated with battery capacity degradation, to train a deep learning model. Therefore, this paper compares the performance of the proposed method with the conventional method using only the peaks and valleys of the DTV curve. The SOH estimation results for the LCO/NCO battery and NCM/NCA battery data sets are shown in Fig. 12 and Table 4. The proportion of training data and test data for SOH estimation is 6:4.
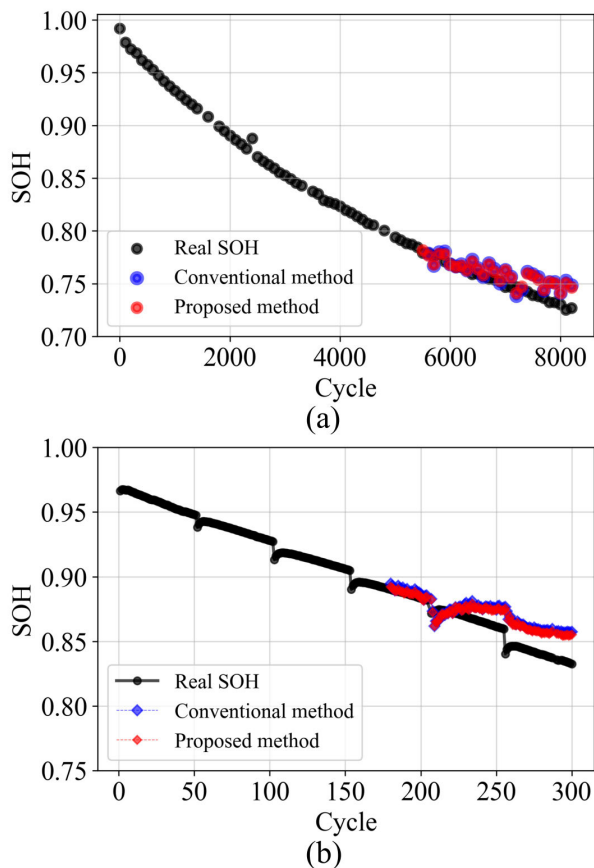
FIGURE 12. Comparison of SOH estimation performance between the conventional method and the proposed method: (a) LCO/NCO battery, (b) NCM/NCA battery.

TABLE 5. Estimation error according to data split proportions.

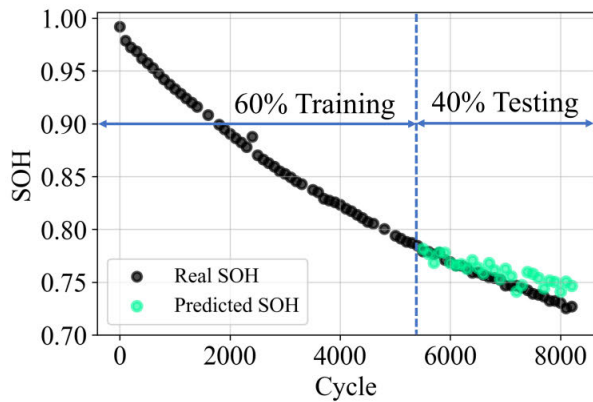| Battery type	Data split proportions	MAE	RMSE
LCO/NCO	6:4	0.00882	0.01146
	7:3	0.007881	0.009527
	8:2	0.005644	0.006715
NCM/NCA	6:4	0.009407	0.01168
	7:3	0.008002	0.009218
	8:2	0.002699	0.004855

SOH estimation performance because the LSTM model was trained by additionally introducing good quality HIs.

The amount of training data may vary depending on the size of the collected data, which can affect the model's performance. In this paper, the SOH estimation performance according to the data split proportion was further analyzed. The results are shown in Fig. 13 and Fig. 14. The training data split proportions of the two battery data sets are set as 6:4, 7:3, and 8:2. The estimated performance according to the corresponding proportion is shown in Table 5. When 80% of the training data was used, it can be confirmed that SOH is estimated with high accuracy because learning is performed for various patterns. When 60% of the training data was utilized, the estimation performance was slightly lower than that of 80%, but it still showed good performance with an MAE of 0.0082. This is because integral-based HIs were added to learn various patterns, and overfitting was prevented through the dropout method. These results confirm that the proposed method can achieve high performance even with a small data split proportion for training.
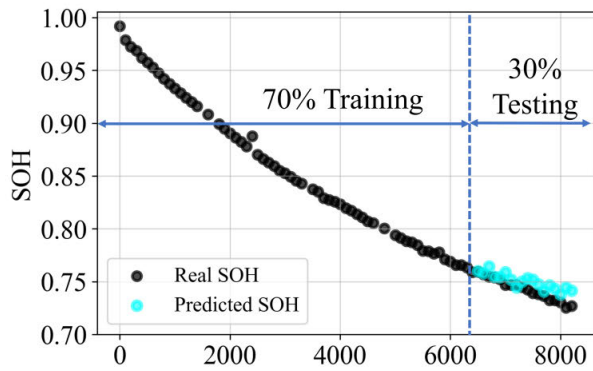
D. DISCUSSION AND FUTURE WORK

In the proposed method, the LSTM model was trained by extracting the integral value of the DTV curve as HIs in the CC charging of the LCO/NCO battery and NCM/NCA battery. DTV curves can be easily derived using simple temperature measurements without additional hardware such as electrochemical impedance spectroscopy (EIS). The proposed method is also readily applicable to real-world applications since CC-CV charging is a standard protocol for Li-ion batteries. Generally, the CC charging current in normal charging mode does not exceed 1C rate, and the LCO/NCO battery and NCM/NCA battery cases studied in this paper were charged at 1C rate and 0.5C rate, respectively. This means the proposed method can be easily implemented and effectively estimate SOH.

But there are still limitations. First, in real applications, data measured by sensors contains noise. Analysis techniques based on incremental calculations, such as ICA and DTV, are significantly affected by noise due to differential operations. In this study, the noise was effectively removed through an SG filter, but the estimation performance may deteriorate depending on the performance of the filter; hence, great care must be taken in filter design. Second, deep learning

Fig. 12(a) is the SOH estimation result of the LCO/NCO battery. The blue dot represents the SOH estimation performance of the LSTM model trained using only the peak and valley information of the DTV curve. As in the existing literature, for the LSTM model trained using only the position and height of the peak and valley of the DTV curve as HIs, the MAE was 0.009978, and the RMSE was 0.01274. However, for the LSTM model trained by additionally using the integral value of the DTV curve as proposed in this paper, the MAE is 0.00882, and the RMSE is 0.01146. Fig. 12(b) is the SOH estimation result of the NCM/NCA battery. As with the LCO/NCO battery, the blue dot represents the SOH estimation performance of the LSTM model trained using only the peak and valley information of the DTV curve. For the existing method, the MAE was 0.01172, and the RMSE was 0.01415. The SOH estimation performance of the proposed method is MAE of 0.01038 and RMSE of 0.01288.

By additionally utilizing the integral value of the DTV curve over a specific voltage range as HI, the MAE was reduced by 11.6% and the RMSE by 10.01% for the LCO/NCO battery. In the case of the NCM/NCA battery, MAE decreased by 11.43%, and RMSE decreased by 8.98%. The proposed method achieved more accurate

FIGURE 13. SOH estimation results according to data proportion ratio of LCO/NCO battery: (a) 6:4 proportion of dataset, (b) 7:3 proportion of dataset (c) 8:2 proportion of dataset.

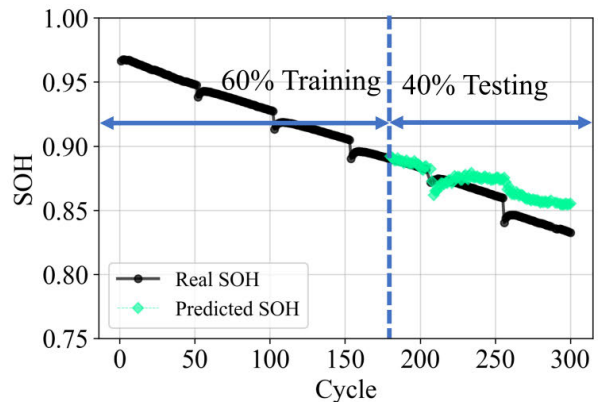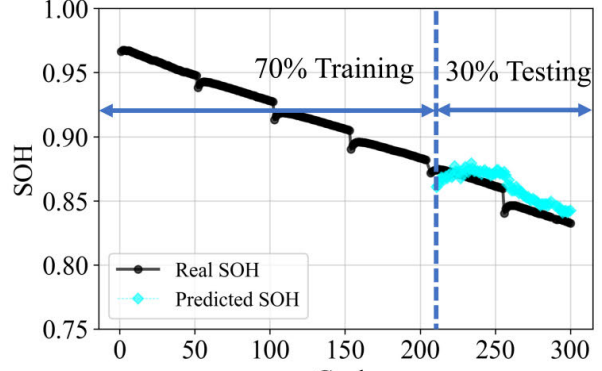**FIGURE 14.** SOH estimation results according to data proportion ratio of NCM/NCA battery: (a) 6:4 proportion of dataset, (b) 7:3 proportion of dataset (c) 8:2 proportion of dataset.
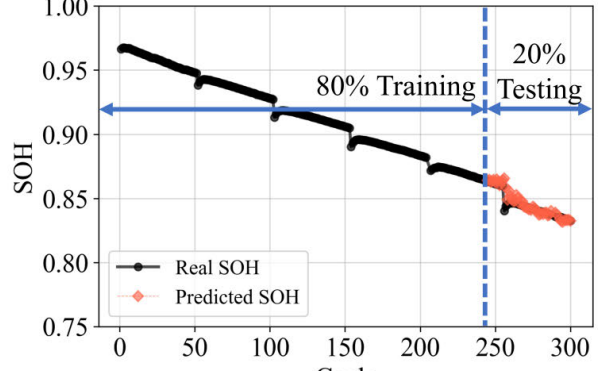
models trained with specific batteries and environments can only be applied under the same conditions [33]. Different types of battery packs are used in real-world applications, and the DTV curve may vary accordingly. Additionally, the DTV curve may change depending on the outside temperature. Therefore, it is necessary to build an extensive database for various batteries and temperatures to apply it to practical applications. Lastly, additional verifications of various charging protocols are required. Typically, ICA and DTV are extracted under CC charging conditions. However,

recently, in the case of electric vehicles (EVs), various fast charging techniques have been proposed to solve the problem of long charging times [34], [35]. When the current profile changes during charging, such as pulse charging (PC) and multistage constant current- constant voltage (MCC-CV) charging, the battery voltage and temperature also change. To the author's knowledge, no literature extracts and analyzes DTV curves for these various charging techniques.

As explained above, many challenges remain in applying the proposed method to practical applications. The authors

plan to build large-scale datasets from different battery models and environmental conditions for SOH estimation in future work. These are expected to provide a basis for applying the proposed method to various battery models and environmental conditions.

V. CONCLUSION

In this research, the differential thermal voltammetry curve was analyzed using the degradation data of the LCO/NCO battery and the NCM/NCA battery, and the state of health estimation method based on this was studied. A differential thermal voltammetry curve was extracted using battery voltage and temperature data obtained under constant current charging conditions, and the calculated peak, valley, and integral values were selected as health indicators. The chosen health indicators were used to train a deep learning model, and the existing and proposed methods were compared. The summary and main contributions of this paper are as follows:

1) To analyze the differential thermal voltammetry curves of various batteries, two battery datasets consisting of cathode materials of LCO/NCO and NCM/NCA, respectively, were used;

2) Noise was removed based on the Savitzky-Golay filter to extract accurate differential thermal voltammetry curves and health indicators;

3) The peak, valley, and integral value calculated during the battery degradation process were selected as HIs,

4) Pearson correlation analysis was used to quantitatively analyze the correlation between the extracted health indicators and battery capacity, and it was verified that integral-based health indicators have a high correlation with capacity degradation;

5) When integral-based Health indicators were added and used as input to Long short-term memory, mean absolute error decreased by 11.6%, and Root mean square error decreased by up to 10.01%. It is also confirmed that high accuracy can be achieved even with small training data.

In conclusion, this study verifies that the proposed method can improve the performance of state of health estimation based on differential thermal voltammetry.

REFERENCES

[1] X. Han, M. Ouyang, L. Lu, J. Li, Y. Zheng, and Z. Li, "A comparative study of commercial lithium ion battery cycle life in electrical vehicle: Aging mechanism identification," *J. Power Sources*, vol. 251, pp. 38–54, Apr. 2014.

[2] L. Cai, J. Meng, D.-I. Stroe, G. Luo, and R. Teodorescu, "An evolutionary framework for lithium-ion battery state of health estimation," *J. Power Sources*, vol. 412, pp. 615–622, Feb. 2019.

[3] M. Winter, B. Barnett, and K. Xu, "Before Li ion batteries," *Chem. Rev.*, vol. 118, no. 23, pp. 11433–11456, Nov. 2018.

[4] N. Lyu, Y. Jin, R. Xiong, S. Miao, and J. Gao, "Real-time overcharge warning and early thermal runaway prediction of Li-ion battery by online impedance measurement," *IEEE Trans. Ind. Electron.*, vol. 69, no. 2, pp. 1929–1936, Feb. 2022.

[5] Z. Chen, M. Sun, X. Shu, R. Xiao, and J. Shen, "Online state of health estimation for lithium-ion batteries based on support vector machine," *Appl. Sci.*, vol. 8, no. 6, p. 925, Jun. 2018.

[6] X. Meng, Y. Xu, H. Cao, X. Lin, P. Ning, Y. Zhang, Y. G. Garcia, and Z. Sun, "Internal failure of anode materials for lithium batteries—A critical review," *Green Energy Environ.*, vol. 5, no. 1, pp. 22–36, Jan. 2020.

[7] N. Lotfi, J. Li, R. G. Landers, and J. Park, "Li-ion battery state of health estimation based on an improved single particle model," in *Proc. Amer. Control Conf. (ACC)*, Seattle, WA, USA, May 2017, pp. 86–91.

[8] N. A. Azis, E. Joelianto, and A. Widyotriatmo, "State of charge (SoC) and state of health (SoH) estimation of lithium-ion battery using dual extended Kalman filter based on polynomial battery model," in *Proc. 6th Int. Conf. Instrum., Control, Autom. (ICA)*, Bandung, Indonesia, Jul. 2019, pp. 88–93.

[9] X. Hu, H. Yuan, C. Zou, Z. Li, and L. Zhang, "Co-estimation of state of charge and state of health for lithium-ion batteries based on fractional-order calculus," *IEEE Trans. Veh. Technol.*, vol. 67, no. 11, pp. 10319–10329, Nov. 2018.

[10] Z. Deng, X. Hu, P. Li, X. Lin, and X. Bian, "Data-driven battery state of health estimation based on random partial charging data," *IEEE Trans. Power Electron.*, vol. 37, no. 5, pp. 5021–5031, May 2022.

[11] Z. Deng, L. Xu, H. Liu, X. Hu, B. Wang, and J. Zhou, "Rapid health estimation of in-service battery packs based on limited labels and domain adaptation," *J. Energy Chem.*, vol. 89, pp. 345–354, Feb. 2024.

[12] T. Qin, S. Zeng, and J. Guo, "Robust prognostics for state of health estimation of lithium-ion batteries based on an improved PSO-SVR model," *Microelectron. Rel.*, vol. 55, nos. 9–10, pp. 1280–1284, Aug. 2015.

[13] Y. Zhang, R. Xiong, H. He, and M. G. Pecht, "Long short-term memory recurrent neural network for remaining useful life prediction of lithium-ion batteries," *IEEE Trans. Veh. Technol.*, vol. 67, no. 7, pp. 5695–5705, Jul. 2018.

[14] Z. Deng, X. Hu, X. Lin, L. Xu, Y. Che, and L. Hu, "General discharge voltage information enabled health evaluation for lithium-ion batteries," *IEEE/ASME Trans. Mechatronics*, vol. 26, no. 3, pp. 1295–1306, Jun. 2021.

[15] R. R. Richardson, C. R. Birkl, M. A. Osborne, and D. A. Howey, "Gaussian process regression for in situ capacity estimation of lithium-ion batteries," *IEEE Trans. Ind. Informat.*, vol. 15, no. 1, pp. 127–138, Jan. 2019.

[16] R. Xiong, Y. Zhang, J. Wang, H. He, S. Peng, and M. Pecht, "Lithium-ion battery health prognosis based on a real battery management system used in electric vehicles," *IEEE Trans. Veh. Technol.*, vol. 68, no. 5, pp. 4110–4121, May 2019.

[17] L. Zheng, J. Zhu, D. D.-C. Lu, G. Wang, and T. He, "Incremental capacity analysis and differential voltage analysis based state of charge and capacity estimation for lithium-ion batteries," *Energy*, vol. 150, pp. 759–769, May 2018.

[18] Z. Wang, J. Ma, and L. Zhang, "State-of-Health estimation for lithium-ion batteries based on the multi-island genetic algorithm and the Gaussian process regression," *IEEE Access*, vol. 5, pp. 21286–21295, 2017.

[19] Y. Merla, B. Wu, V. Yufit, N. P. Brandon, R. F. Martinez-Botas, and G. J. Offer, "Novel application of differential thermal voltammetry as an in-depth state-of-health diagnosis method for lithium-ion batteries," *J. Power Sources*, vol. 307, pp. 308–319, Mar. 2016.

[20] E. Schaltz, D.-I. Stroe, K. Nørregaard, L. S. Ingvardsen, and A. Christensen, "Incremental capacity analysis applied on electric vehicles for battery State-of-Health estimation," *IEEE Trans. Ind. Appl.*, vol. 57, no. 2, pp. 1810–1817, Mar. 2021.

[21] Y. Li, M. Abdel-Monem, R. Gopalakrishnan, M. Berecibar, E. Nanini-Maury, N. Omar, P. van den Bossche, and J. Van Mierlo, "A quick on-line state of health estimation method for Li-ion battery with incremental capacity curves processed by Gaussian filter," *J. Power Sources*, vol. 373, pp. 40–53, Jan. 2018.

[22] Z. Wang, C. Yuan, and X. Li, "Lithium battery state-of-health estimation via differential thermal voltammetry with Gaussian process regression," *IEEE Trans. Transport. Electrific.*, vol. 7, no. 1, pp. 16–25, Mar. 2021.

[23] L. Zhang, W. Wang, H. Yu, Z. Zhang, X. Yang, F. Liang, S. Li, S. Yang, and X. Liu, "Remaining useful life and state of health prediction for lithium batteries based on differential thermal voltammetry and a deep learning model," *iScience*, vol. 25, no. 12, Dec. 2022, Art. no. 105638.

[24] X. Yang, B. Ma, H. Xie, W. Wang, B. Zou, F. Liang, X. Hua, and S. Chen, "Lithium-ion battery state of health estimation with multi-feature collaborative analysis and deep learning method," *Batteries*, vol. 9, no. 2, p. 120, Feb. 2023.

[25] W. Wang, L. Zhang, H. Yu, X. Yang, T. Zhang, S. Chen, F. Liang, H. Wang, X. Lu, S. Yang, and X. Liu, "Early prediction of the health conditions for battery cathodes assisted by the fusion of feature signal analysis and deep-learning techniques," *Batteries*, vol. 8, no. 10, p. 151, Oct. 2022.

[26] B. Ma, S. Yang, L. Zhang, W. Wang, S. Chen, X. Yang, H. Xie, H. Yu, H. Wang, and X. Liu, "Remaining useful life and state of health prediction for lithium batteries based on differential thermal voltammetry and a deep-learning model," *J. Power Sources*, vol. 548, Nov. 2022, Art. no. 232030.

[27] A. Krupp, E. Ferg, F. Schuldt, K. Derendorf, and C. Agert, "Incremental capacity analysis as a state of health estimation method for lithium-ion battery modules with series-connected cells," *Batteries*, vol. 7, no. 1, p. 2, Dec. 2020.

[28] T. Plattard, N. Barnel, L. Assaud, S. Franger, and J.-M. Duffault, "Combining a fatigue model and an incremental capacity analysis on a commercial NMC/graphite cell under constant current cycling with and without calendar aging," *Batteries*, vol. 5, no. 1, p. 36, Mar. 2019.

[29] B. Christoph. (2017). *Oxford Battery Degradation Dataset 1*. Univ. Oxford, Oxford, U.K. [Online]. Available: https://ora.ox.ac.uk/objects/uuid:03ba4b01-cfed-46d3-9b1a-7d4a7bdf6fac

[30] S. Maleki, B. Ray, and M. T. Hagh, "Hybrid framework for predicting and forecasting state of health of lithium-ion batteries in electric vehicles," *Sustain. Energy, Grids Netw.*, vol. 30, Jun. 2022, Art. no. 100603.

[31] L. Wang, S. Qiao, D. Lu, Y. Zhang, C. Pan, Z. He, X. Zhao, and R. Wang, "State of health estimation of lithium-ion battery in wide temperature range via temperature-aging coupling mechanism analysis," *J. Energy Storage*, vol. 47, Mar. 2022, Art. no. 103618.

[32] X. Li, C. Yuan, and Z. Wang, "Multi-time-scale framework for prognostic health condition of lithium battery using modified Gaussian process regression and nonlinear regression," *J. Power Sources*, vol. 467, Aug. 2020, Art. no. 228358.

[33] J. He, Z. Wei, X. Bian, and F. Yan, "State-of-Health estimation of lithium-ion batteries using incremental capacity analysis based on voltage–capacity model," *IEEE Trans. Transport. Electrific.*, vol. 6, no. 2, pp. 417–426, Jun. 2020.

[34] H. Bizhani, S. K. H. Sani, H. Rezazadeh, S. M. Muyeen, and S. Rahmani, "Modeling of an optimum fast charging multi-step constant current profile for lead-acid batteries," *IEEE Trans. Ind. Appl.*, vol. 59, no. 2, pp. 2050–2060, Mar. 2023.

[35] K. K. Duru, C. Karra, P. Venkatachalam, S. A. Betha, A. A. Madhavan, and S. Kalluri, "Critical insights into fast charging techniques for lithium-ion batteries in electric vehicles," *IEEE Trans. Device Mater. Rel.*, vol. 21, no. 1, pp. 137–152, Mar. 2021.
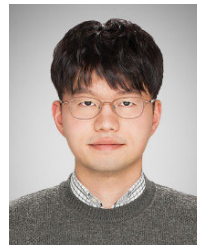
JAEJUNG YUN (Member, IEEE) received the Ph.D. degree in electrical engineering from Pohang University of Science and Technology, Pohang, South Korea, in 2012.

He was a Senior Researcher with the Samsung Advanced Institute of Technology (SAIT), Suwon, South Korea, where he involved in developing power conversion systems for electric vehicles and renewable energy. He is currently an Assistant Professor with the School of Electrical Engineering, Chungbuk National University, Cheongju-si, South Korea. His research interests include battery management systems, the design and control of power conversion systems, and wireless power transfer systems.

YEONHO CHOI was born in Cheonan, South Korea, in January 1997. He received the B.S. degree in electrical engineering from Chungbuk National University, Cheongju, South Korea, in 2022, where he is currently pursuing the combined master's and Ph.D. degree with the School of Electrical Engineering. His research interests include battery management systems and state estimation algorithm.

PAUL JANG (Member, IEEE) received the B.S. and Ph.D. degrees in electrical engineering from Seoul National University, Seoul, South Korea, in 2010 and 2017, respectively. He was a Senior Researcher with the Samsung Electronics Digital Media and Communications (DMC) Research and Development Center, Seoul, where he involved in developing a wireless power transfer system for consumer electronics. He is currently an Associate Professor with the Department of Energy and Electrical Engineering, Tech University of Korea, Siheung-si, South Korea. His research interests include modular converter systems, distributed power systems, and soft-switching converters.

• • •